AAS 13-493

TOUR DESIGN USING RESONANT ORBIT HETEROCLINIC CONNECTIONS IN PATCHED CIRCULAR RESTRICTED THREE-BODY PROBLEMS

Rodney L. Anderson*

It is increasingly desirable to incorporate multi-body effects in tour design early in the process to make use of these effects and potentially discover new solutions. Flybys have previously been designed using the heteroclinic connections of resonant orbits in the circular restricted three-body problem (CRTBP), but tour design often requires the consideration of additional moons, especially within the Jovian system. In this study, the heteroclinic connections of multiple resonant orbits are chained together within separate CRTBP models to perform multiple flybys that advance through desired resonances. The aspects of patching these trajectories together are explored, and sample trajectories are computed.

INTRODUCTION

It has become increasingly desirable to include multi-body effects early in the process of designing a tour with multiple flybys. Including these effects from the beginning of the process allows the trajectory to take full advantage of these multi-body effects and incorporate alternatives that are not necessarily apparent when using two-body techniques alone. Patched-conic techniques are often used to design tours with two-body techniques, and some researchers have begun to include three-body effects in the analysis in the form of Tisserand's criterion[1–3] or Tisserand graphs.[4]

Dynamical systems theory has also been applied to the design of Earth-Moon transfers in the three-body problem,[5] and unstable resonant orbits have been a component of some of these techniques.[6] Another area of interest has been in understanding the resonance transition of comets, which have been explained from the perspective of weak stability boundaries[7] and the use of heteroclinic connections of libration orbits.[8–10] Lantoine, Russell, and Campagnola found the computation of resonant orbits themselves to be useful as inputs to optimization algorithms without invariant manifolds.[11] Ross and Scheeres also showed that an energy kick function could be used to approximate the effect of a gravity flyby.[12]

The use of heteroclinic connections of unstable resonant orbits has laid the foundation for the techniques used in this study. Early work by Anderson and Lo showed that ballistic trajectories,[13] impulsive trajectories originally designed using two-body techniques,[14–16] and optimized low-thrust trajectories[17,18] follow the invariant manifolds of these unstable resonant orbits. The computation of homoclinic[19] and heteroclinic[13] connections of these unstable resonant orbits were shown to be an important tool for computing resonance transition, and these techniques were used to compute trajectories with multiple resonance transitions for the endgame problem in the Jupiter-Europa system.[20] Work comparing the convergence of optimized solutions for a single resonance transition has shown at least an order of magnitude improvement in the convergence when using heteroclinic connection initial guesses versus resonant orbits alone.[21] In this case using resonant orbits already gave a significant improvement over patched-conic methods in terms of the speed of convergence. The invariant manifolds of resonant orbits have been shown to be useful for computing the final approach[22,23] although that element will not be included in this analysis. Vaquero and Howell have also

*Member of Technical Staff, Jet Propulsion Laboratory, California Institute of Technology, 4800 Oak Grove Drive, M/S 301-121, Pasadena, CA 91109

used these heteroclinic connections of resonant orbits to study resonance transition, and they have employed similar techniques to examine resonance transition using three-dimensional resonant orbits.[24–26]

Many of the components required for the design of a complete tour using dynamical systems techniques and the heteroclinic connections of unstable resonant orbits have now been analyzed. The approach problem has been characterized,[22,23] and the ability to compute a trajectory traveling through multiple resonances in a single system via heteroclinic connections of resonant orbits has been established.[20] The transition of comets between exterior and interior resonances in a three-body system using the heteroclinic connection of libration orbits has also previously been examined.[8–10] The focus of this study is to explore methods for patching trajectories in different circular restricted three-body (CRTBP) systems together. Specifically the stable and unstable manifolds of unstable resonant orbits will be used to form the connections between interior resonant orbits in one system and exterior resonant orbits in another system. As Europa has been the focus of prior studies, the transition between the Jupiter-Ganymede system and the Jupiter-Europa system will be taken as a test case for this study. The focus here will be on exploring the design of trajectories using these techniques and discussing the various factors and trades that come into play when designing these types of trajectories. Some aspects of how these techniques can be incorporated into the total trajectory design process will be discussed and trajectories such as those needed for eventual integration into a continuous tour will be generated.

BACKGROUND

Circular Restricted Three-Body Problem

The circular restricted three-body problem (CRTBP) provides the framework for this study. The trajectories computed in this model are used as the basis for the final trajectory found when the CRTBPs are patched together. Szebehely[27] provides the details of the model in a different form, but the basic equations are given here. In this model, a spacecraft is modeled as an infinitesimal mass moving in a system with two massive bodies orbiting one another in circular orbits. A rotating frame may be aligned with these two bodies with the x axis pointing from the larger body (the primary) to the smaller body (the secondary). The y axis points in the direction of motion of the secondary, and the z axis completes the right-handed coordinate frame. The mass of the larger primary is $1-\mu$, and the mass of the secondary is μ. Then the primary is located at $x=-\mu$, and the secondary is located at $x=1-\mu$. The values of μ used in this study are listed in Table 1. The equations of motion of the infinitesimal mass may be written in the rotating frame as

Table 1. Mass ratios for the Jupiter-Europa and Jupiter-Ganymede CRTBP systems

System	μ
Jupiter-Europa	0.0000252664488504
Jupiter-Ganymede	0.0000780369094055

$$\begin{aligned} \ddot{x}-2\dot{y} &= \frac{\partial \Omega}{\partial x} \\ \ddot{y}+2\dot{x} &= \frac{\partial \Omega}{\partial y} \\ \ddot{z} &= \frac{\partial \Omega}{\partial z} \end{aligned} \tag{1}$$

where

$$\Omega = \frac{x^2+y^2}{2} + \frac{(1-\mu)}{r_1} + \frac{\mu}{r_2} \tag{2}$$

and

$$r_1 = \sqrt{(x+\mu)^2+y^2+z^2},\ r_2 = \sqrt{(x-1+\mu)^2+y^2+z^2}. \tag{3}$$

Five equilibrium points are found in the problem with three collinear equilibrium points located on the $y = 0$ line and two triangular equilibrium points that are equidistant from the primary and the secondary. A constant of motion (the Jacobi constant) is also found in the problem, and it may be written as

$$\mathrm{C} = 2\Omega - \mathrm{V}^2 = x^2 + y^2 + \frac{2(1-\mu)}{r_1} + \frac{2\mu}{r_2} - \dot{x}^2 - \dot{y}^2 - \dot{z}^2. \tag{4}$$

Libration orbits found around the equilibrium points and resonant orbits may both be computed using one of the symmetry properties of the CRTBP.[28,29] The particular property of interest here states that if an orbit intersects the xz plane perpendicular to the plane in two different points, the orbit will be a symmetric, periodic orbit. This property forms the basis of a single-shooting algorithm[30] that uses the variational equations to update an initial guess for an orbit until a periodic orbit is obtained. An adaptation of this algorithm is used to compute the resonant orbits in this study.

Unstable periodic orbits possess both stable and unstable manifolds. Stable (unstable) manifolds may be thought of as those trajectories that approach the unstable periodic orbit as time goes to ∞ ($-\infty$). Formally, the definition for the stable and unstable manifolds of a flow ϕ_t with a limit set (L) are

Stable Manifold $W^s(L)$: The set of points x such that $\phi_t(x)$ approaches L as $t \to \infty$.

Unstable Manifold $W^u(L)$: The set of points x such that $\phi_t(x)$ approaches L as $t \to -\infty$.

The invariant manifolds are globalized here using an offset of approximately 1×10^{-6} dimensionless units.[31] Refer to Wiggins for more details on invariant manifolds.[32]

Poincaré Sections

Poincaré maps are used throughout this study as a tool to search for heteroclinic connections. These Poincaré maps are computed by placing a *hypersurface* Σ or surface of section in $\mathbb{R}^{n-1}$ transverse to the flow. In this study within the planar CRTBP, the hypersurface is defined by $y = 0$ with $x < 0$. In each case a trajectory is integrated until it intersects the hypersurface, and the mapping is from one intersection to the next. When x and $\dot{x}$ are used to plot the Poincaré section for a given Jacobi constant, $\dot{y}$ may be computed from a point in the section as

$$\dot{y} = \pm\sqrt{x^2 + y^2 + \frac{2(1-\mu)}{r_1} + \frac{2\mu}{r_2} - \dot{x}^2 - C}. \tag{5}$$

One-sided Poincaré maps for this case only contain those points traveling in either $+\dot{y}$ or $-\dot{y}$.

Heteroclinic Connections

Heteroclinic and homoclinic trajectories are computed from intersections of the stable and unstable manifolds. A heteroclinic trajectory may be defined as a point that belongs to

$$W^s_{a:b} \cap W^u_{c:d} \tag{6}$$

where in the notation used here, a:b and c:d designate which resonant orbit was used to compute the invariant manifolds. Given a heteroclinic connection, the trajectory travels backward in time asymptotically along the unstable manifold to one resonant orbit and asymptotically forward in time along the stable manifold to the other resonant orbit. A homoclinic trajectory is defined as a point that belongs to

$$W^s_{a:b} \cap W^u_{a:b}, \tag{7}$$

and the trajectory approaches the same unstable resonant orbit asymptotically both forward and backward in time. For the trajectories designed here, heteroclinic connections will be used to connect resonant orbits at the same energy in the same system.

UNSTABLE RESONANT ORBITS

As described earlier, unstable resonant orbits are the foundational elements of the techniques used for the development of trajectories in this study. For a Keplerian orbit, a spacecraft would travel around the primary an integer number of times (p) while the secondary travels around the primary an integer number of times (q). In the three-body problem, the spacecraft is perturbed by the secondary, and the relationship between the revolutions becomes approximate: $pn_p \approx qn_q$. Here, the mean motion of the secondary (n_q) is one in the CRTBP, and the mean motion of the spacecraft is $n_p = p/q$. Resonant orbits in this case may be found using a variety of techniques including numerical searches and Poincaré sections. The resonance is commonly estimated for mission design purposes using the osculating two-body period of the orbit far from the secondary. The notation used in this study for designating the resonance of a selected orbit is [spacecraft revolutions]:[body revolutions], a convention commonly found in dynamical astronomy and astrodynamics literature.[33,34] (Note that the reverse notation may also be found in some studies.) See Murray and Dermott[33] for a more detailed explanation of resonance in general or Anderson and Lo[16] for additional information on how it is used in this context.

In general a tour can include transitions between interior resonant orbits (those trajectories with periods smaller than that of the secondary around the primary) and exterior resonant orbits (those trajectories with periods greater than that of the system). A sample of three interior resonant orbits that are useful for this

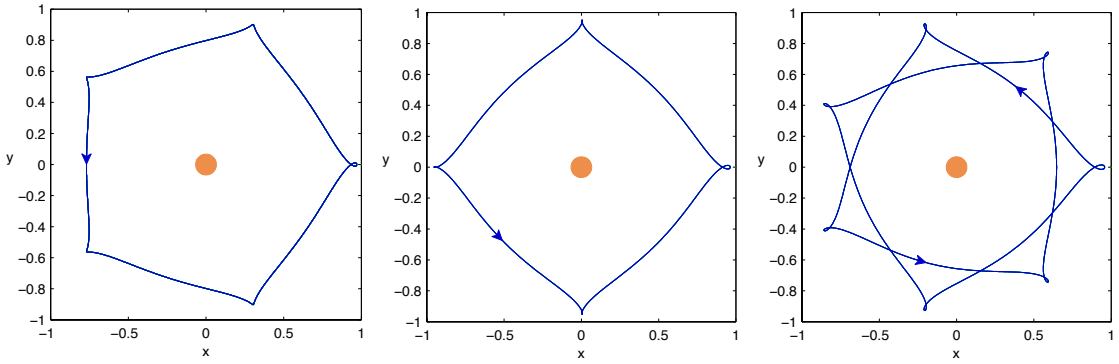

(a) 5:4 Resonant Orbit (b) 4:3 Resonant Orbit (c) 7:5 Resonant Orbit

Figure 1. Resonant orbit sequence in the Jupiter-Ganymede rotating frame using interior resonant orbits at C = 3.0068.

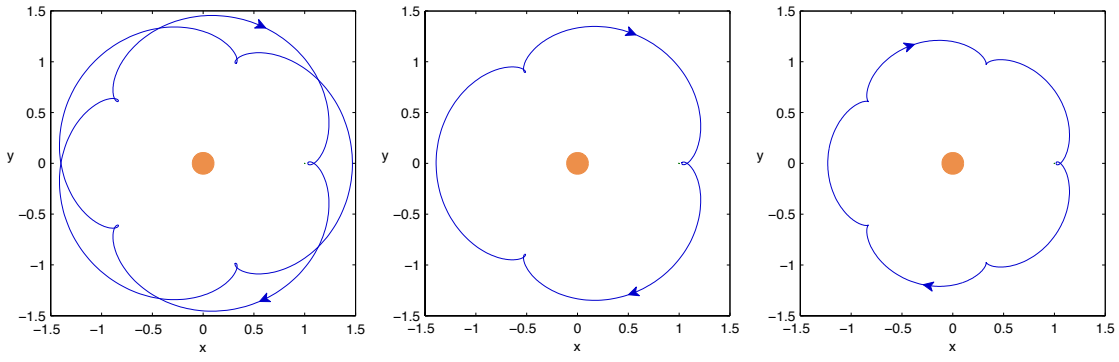

(a) 5:7 Resonant Orbit (b) 3:4 Resonant Orbit (c) 5:6 Resonant Orbit

Figure 2. Resonant orbit sequence in the Jupiter-Europa rotating frame using exterior resonant orbits at C = 3.002459523649998.

study are shown in Figure 1 in the Jupiter-Ganymede rotating frame for C = 3.0068. Three exterior resonant orbits in the Jupiter-Europa system for C = 3.002459523649998 are given in Figure 2. Note that this value of C is the same as C_f used for the final approach of the planar Europa orbiter analyzed in Anderson and Lo,[16] and it is a good first estimate of the Jacobi constant that might be targeted for a final approach to Europa at the end of the endgame scenario. As can be seen in several of the orbits, small loops develop at particular points on the orbit. For exterior (interior) orbits these correspond to the points where the spacecraft is traveling faster (slower) than the secondary around the primary. Additional resonant orbits are also considered in this study, but they generally have the same features as the orbits shown here. The majority of the resonant orbits used here are continued from $\mu = 0$ to the desired μ, and the generating orbits are classified as first species, second kind.[35] Occasionally a resonant orbit found via a numerical search is also included.

RESONANT PATHWAY SELECTION

Selecting an optimal sequence of resonances is still an area of active research, and the optimal sequence will of course depend on the constraints and objectives of the mission. A number of sequences have been found to consistently exist as solutions to particular problems. For example, the final approach to Europa in a tour design commonly includes a transition from the 3:4 to the 5:6 resonance, perhaps with an intermediate resonance inserted. An additional factor in the design of each case is the Jacobi constant at which the resonance transitions takes place. For the Europa endgame scenario, Anderson and Lo[20] examined 5:7 – 3:4 – 7:9 – 5:6 and 7:10 – 3:4 – 5:6 sequences among others in the Jupiter-Europa system.

One benchmark problem in the literature is to examine a trajectory traveling from a resonance close to Ganymede to another resonance close to Europa.[11,36] Lantoine, Russell, and Campagnola[11] connect a sequence of resonances with C = 3.0068 in the Jupiter-Ganymede system to a sequence of resonances at C = 3.0024 in the Jupiter-Europa system. It is expected from previous studies that a transfer will exist at these energies,[36] and the final energy is close to that of the final approach energy for the planar Europa orbiter (C_f). They examined a number of different resonant sequences with one of the shortest using a 5:4 – 4:3 – 7:5 sequence in the Jupiter-Ganymede system followed by a 5:7 – 3:4 – 7:9 – 5:6 sequence in the Jupiter-Europa system. In their case they used an algorithm that took the resonant orbits themselves as initial guesses and numerically optimized the trajectory to find a solution. In this case, the Jacobi constants of the converged segments may vary based on the placement of the maneuvers. This variability will be a factor in the following analysis.

In this study, similar resonant pathways will be explored so as to allow an easier comparison to prior work, but other sequences of resonances are certainly possible. The focus here will be on the transition from interior resonant orbits in one system to exterior resonant orbits in another system, but these techniques are also not limited to transitions in this direction. A Jacobi constant of C = 3.0068 will generally be used in the Jupiter-Ganymede system, and a Jacobi constant of C = 3.0024 or C = C_f will generally be targeted for the Jupiter-Europa system.

SELECTING THE INTERSECTION TO PATCH THE CRTBPS

Many trajectories transitioning between the Jupiter-Ganymede system and the Jupiter-Europa system appear to use something similar to a transition between a 7:5 interior orbit in the Jupiter-Ganymede system and a 5:7 exterior orbit in the Jupiter-Europa system, so this sequence will be used to explore the process of patching the two models. A variety of different techniques exist in the literature to patch the trajectories from different three-body systems together. Campagnola and Russell[3] use a Tisserand-Poincaré graph technique, and Koon et al.[36] use libration point orbits with a method similar to the one employed here. The resulting trajectories are then eventually moved into the coupled three-body model[36–39] or the ephemeris problem. The technique explored here will search for intersections in Poincaré sections directly between the invariant manifolds of unstable resonant orbits in each system. More specifically, $W^u_{7:5}$ at C = 3.0068 will be computed in the Jupiter-Ganymede system, and $W^s_{5:7}$ will be computed at a desired Jacobi constant in the Jupiter-Europa system. A subset of the trajectories on the W^u of the 7:5 Jupiter-Ganymede resonant orbit and the W^s of the 5:7 Jupiter-Europa resonant orbit are plotted in configuration space in Figure 3. In each case their intersec-

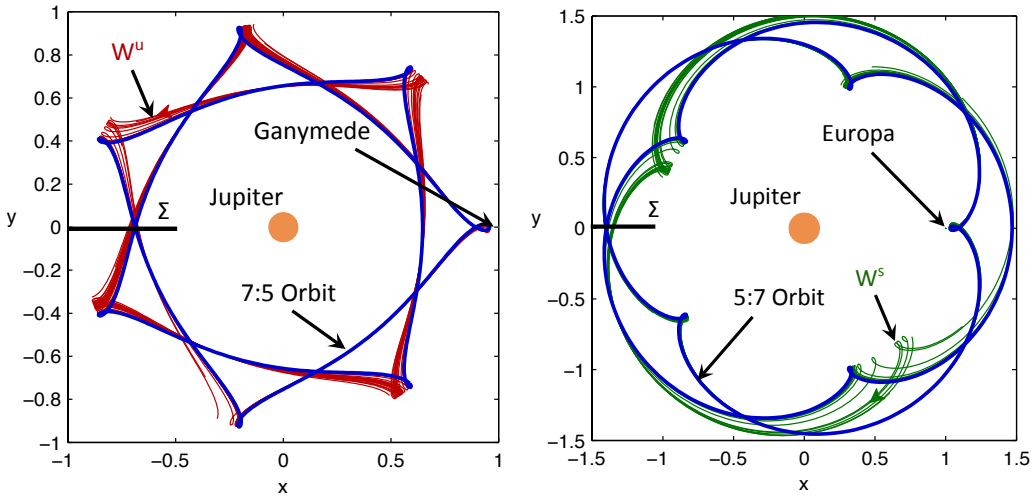

(a) 7:5 Resonant Orbit with W^u at C = 3.0068 in the Jupiter-Ganymede System

(b) 5:7 Resonant Orbit with W^s at C = 3.002459523649998 in the Jupiter-Europa System

Figure 3. Invariant manifold trajectories of selected orbits in the Jupiter-Ganymede and Jupiter-Europa systems.

tions are captured at Σ, and the points may be plotted in a Poincaré section. Note that the trajectories on the invariant manifolds are integrated for longer durations than shown here for the Poincaré sections in order to search for the desired intersections, and a larger number of trajectories are computed.

The Poincaré sections computed for the Jupiter-Ganymede system at C = 3.0068 and the Jupiter-Europa system at C = C_f using Σ as the surface of section are given in Figure 4. Here, the points are plotted in

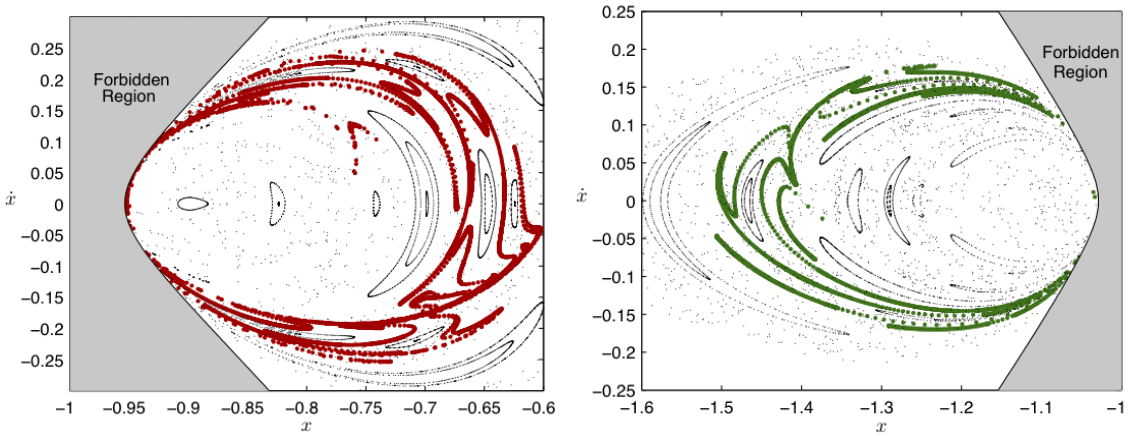

(a) W^u intersections of the 7:5 orbit in the Jupiter-Ganymede System for C = 3.0068

(b) W^s intersections of the 5:7 orbit in the Jupiter-Europa System for C = C_f

Figure 4. Poincaré sections of the desired invariant manifolds in their respective rotating frames

their respective rotating frames, and the forbidden regions are plotted for each Jacobi constant. The number of points used in computing the invariant manifolds are selected based on the competing requirements of computational speed and the accuracy required to compute the desired intersections. Because the 7:5 orbit in the Jupiter-Ganymede system is an interior resonant orbit, the majority, but not all, of the $\dot{y}$ values are

negative. All points regardless of the sign of $\dot{y}$ are plotted here, but limits will be placed on these points when they are compared to the Jupiter-Europa Poincaré section points. The majority of the $\dot{y}$ values of the points shown in the Jupiter-Europa system are positive because they are computed for an exterior resonant orbit.

To compare the invariant manifold intersections directly and search for a desired intersection, the points in the Poincaré sections need to be transformed to the same coordinates. This can be achieved by converting the coordinates in the Jupiter-Ganymede system to the Jupiter-Europa system or vice versa. It is then assumed that the transition is timed so that the transition between the systems takes place when the surface of sections or the x axes are aligned. The transformation is made with respect to Jupiter as the common point to both systems since the barycenters of each system are at slightly different locations. The transformation for the x coordinate from the Jupiter-Ganymede system to the Jupiter-Europa system may be outlined as follows. In the following, the je subscript indicates a quantity in the Jupiter-Europa frame and jg indicates a quantity in the Jupiter-Ganymede frame. DU is the distance unit required for converting between dimensional and dimensionless quantities, and VU is the velocity unit. Initially x is given in dimensionless, barycentered coordinates. First it may be made dimensional ($x_{jg}DU_{jg}$) and found relative to Jupiter ($x_{jg}DU_{jg} + \mu_{jg}DU_{jg}$). Then it is determined relative to the Jupiter-Europa barycenter and made dimensionless in the rotating Jupiter-Europa frame. If the complete state is transformed in a similar manner then the dimensionless state in the rotating Jupiter-Europa frame may be obtained. See Appendix C of Anderson[19] for more details on the transformation. In each case it is assumed that the rotating and inertial frames are all aligned ($\theta = 0$) in the transformations. Remember that for the particular surface of section selected here, $y_{jg} = 0$, which simplifies the transformation.

Once a desired intersection is found, the nearby points may be used to interpolate and find a more precise intersection in x and $\dot{x}$ coordinates. From this information, it is straightforward to compute the magnitude of $\dot{y} = f(x, y = 0, \dot{x}, C)$ in the system chosen for plotting the Poincaré section. Next, with $y = 0$, x and $\dot{x}$ can be transformed to the other CRTBP system. The magnitude of $\dot{y}$ in this frame may be obtained using the same equation as before with the appropriate C for that system. Finally, the sign of $\dot{y}$ may be chosen from knowledge of the problem or the sign of the points near the intersection. The point may be integrated forward and backward in each system to verify that the trajectory does indeed approach the desired resonant orbit. If it does not, more points may need to be computed to obtain an accurate interpolation. The ΔV required at the patchpoint may be obtained from the dimensional difference in $\dot{y}$ values when they are transformed to a common frame. It should be mentioned that an alternative method might examine the possibility of performing a ΔV in the $\dot{x}$ direction, but it has generally been found that the $\dot{x}$ differences of interest here are very small and difficult to visually discern on the Poincaré section.

The intersections of the invariant manifolds of the resonant orbits with Σ transformed to the Jupiter-Europa rotating frame are shown in Figure 5 for a Jacobi constant of C = 3.0068 (W^u) in the Jupiter-Ganymede system and C = 3.00245952365 (W^s) in the Jupiter-Europa system. Again, the Jacobi constant in the Jupiter-Europa frame has been chosen to be the same as the C used for the final approach in the planar Europa orbiter trajectory developed in Anderson and Lo.[16] The quantities have been converted so that they are all given in the Jupiter-Europa system in the rotating frame. As can be seen in the plot, there are many intersections from which a potential transfer between systems may be computed. The problem now becomes to select the best transfer from among the many possibilities. The two primary criteria used in this selection are the resulting ΔV and the time-of-flight (TOF).

The possible TOFs can first be reduced by limiting the number of intersections with Σ allowed for each trajectory. This criteria is an approximate limitation because in this case the surface of section actually intersects the orbit of interest, unlike some of the cases that are applied to libration orbit trajectories. Therefore, the integration of some invariant manifold trajectories that are initiated just before reaching Σ will be counted as having one intersection before traveling around one time, while those initiated after Σ will not register an intersection until almost one complete revolution. Keep in mind that one additional factor in the TOF is the offset used to globalize the invariant manifolds, but this technique can still eliminate potential trajectories with much longer TOFs. If the number of intersections (n) are limited so that $n \leq 7$ in the Jupiter-Europa system and $n \leq 8$ in the Jupiter-Ganymede system then the plot in Figure 6(a) is obtained. This plot contains several potential intersections, and the number of intersections may be gradually increased to obtain a plot

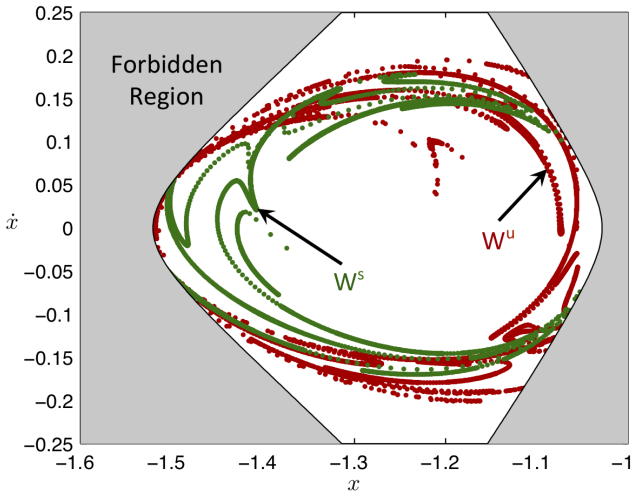

Figure 5. The intersections of the W^s of the 7:5 resonant orbit in the Jupiter-Ganymede system (green) and the W^u of the 5:7 resonant orbit in the Jupiter-Europa system (red). All quantities have been transformed to the Jupiter-Europa system, and it is a one-sided Poincaré map[40] limited to $\dot{y} > 0$. The forbidden regions from both systems are superimposed on the plot because they limit the region of feasible transfers.

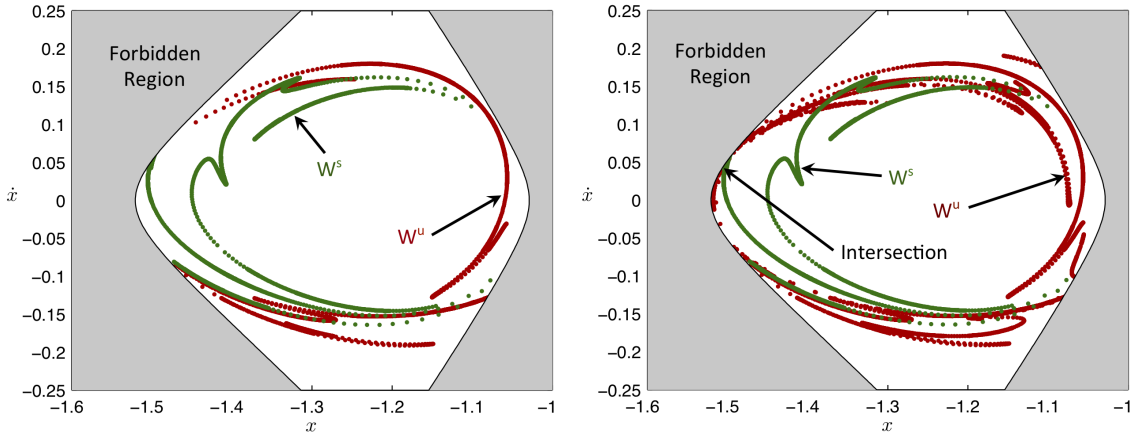

(a) Intersections limited to $n_{jg} \leq 8$ and $n_{je} \leq 7$

(b) Intersections limited to $n_{jg} \leq 10$ and $n_{je} \leq 7$

Figure 6. Poincaré section showing the intersections of the W^s of the 7:5 resonant orbit in the Jupiter-Ganymede system and the W^u of the 5:7 resonant orbit in the Jupiter-Europa system. $n_{jg} \leq 10$ and $n_{je} \leq 7$.

such as that shown in Figure 6(b). This plot has one of the desired intersections (labeled) that will be useful for comparison on the border of one of the forbidden regions with a $\dot{y} > 0$ in the Jupiter-Ganymede frame. This particular point with a Jacobi constant C = C_f has a ΔV = 102.3 m/s.

Another possible variable in the selection of the patchpoint to use in transitioning between the systems is the Jacobi constant used in each system. Often constraints will be imposed that limit the range of acceptable Jacobi constants, but it is worth understanding the trades that occur by exploring the required ΔVs for several other Jacobi constant values. Two additional cases are shown in Figure 7 using C = 3.0024 and C = 3.0 in the Jupiter-Europa system while retaining the same Jacobi constant in the Jupiter-Ganymede system. As can be

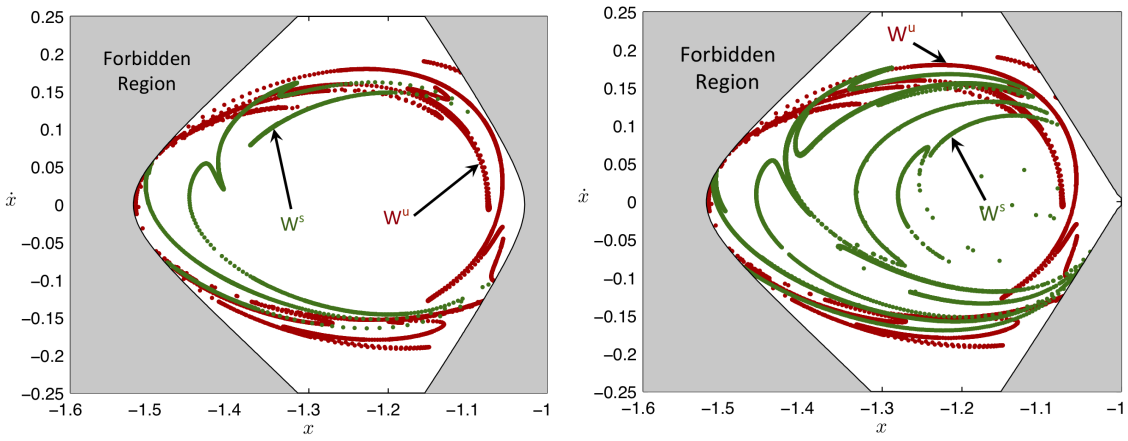

(a) C = 3.0024 in the Jupiter-Europa System

(b) C = 3.0 in the Jupiter-Europa System

Figure 7. Poincaré sections showing the intersections of $W^s_{7:5}$ and $W^u_{5:7}$ transformed into the Jupiter-Europa rotating frame for different Jacobi constants.

seen from the Poincaré section in Figure 7(a), the change from C = C_f to C = 3.0024 is minimal in its overall effect on the invariant manifolds. However, a small change of approximately 0.74 m/s down to 101.6 m/s is seen in the ΔV required to patch the systems together using the patchpoint equivalent to the previously labeled intersection. If a greater jump in the Jacobi constant is applied down to C = 3.0, a more significant decrease in the ΔV for this point down to approximately 76.2 m/s is obtained. The invariant manifold intersections in this case change more significantly as can be seen in the plot. Similar intersections can be observed, but they have moved to different locations in the Poincaré section, and other potential intersections have come into existence. In particular, the intersection of interest has moved to a more negative x and a smaller $\dot{x}$. These new intersections may provide additional options in terms of the necessary ΔV and possible trajectory types to meet mission design constraints. If a different final Jacobi constant is desired, it may still be possible to make use of these options for this leg and change the Jacobi constant on the next leg of the trajectory.

One of the difficulties in selecting an intersection point for transferring between the two systems is determining which point will result in the smallest ΔV. Some more insight may be obtained into the general trends in the ΔV required to patch between the two systems by plotting the theoretical required ΔV for each combination of x and $\dot{x}$ for selected values of the Jacobi constant in each system. In the chosen system for the plot, x, $\dot{x}$, and y are known. With a given value of C, the magnitude of $\dot{y}$ may then be determined, although the sign must still be selected. Most of the intersections of interest for the Jupiter-Europa system are positive, and the Poincaré sections have been limited to $\dot{y} > 0$. In the Jupiter-Ganymede case, the x and $\dot{x}$ coordinates are transferred back to this system, and with $y = 0$, the value of $\dot{y}$ may be determined in this system from the selected Jacobi constant. As previously mentioned, some of the intersections in this system have $\dot{y} > 0$ and some have $\dot{y} < 0$. Plots of the theoretical ΔVs resulting from the two different cases are shown over the possible range of x and $\dot{x}$ values in Figure 8. Now, the intersections in the Poincaré section may be compared to these theoretical values to aid in selecting the intersections with the lowest ΔV.

The question remains as to which plot is appropriate to use for each intersection, and this may be addressed by plotting the invariant manifold intersections color-coded according to the sign of $\dot{y}$ in the Jupiter-Ganymede system with the contoured ΔVs in the background. An example of one way to show this is given in Figure 9. In these plots, the unstable manifolds of the Jupiter-Ganymede 7:5 orbit are shown in both red and orange. Those trajectories with positive $\dot{y}$ in the Jupiter-Ganymede rotating frame at the intersection are shown as red, and those with negative $\dot{y}$ are shown as orange. Figure 9(a) shows contours up to a maximum of 500 m/s for the required ΔV to patch the systems together compared to the actual intersections. As can be seen from the plot, the red points and their intersection with the stable manifold of the Jupiter-Europa

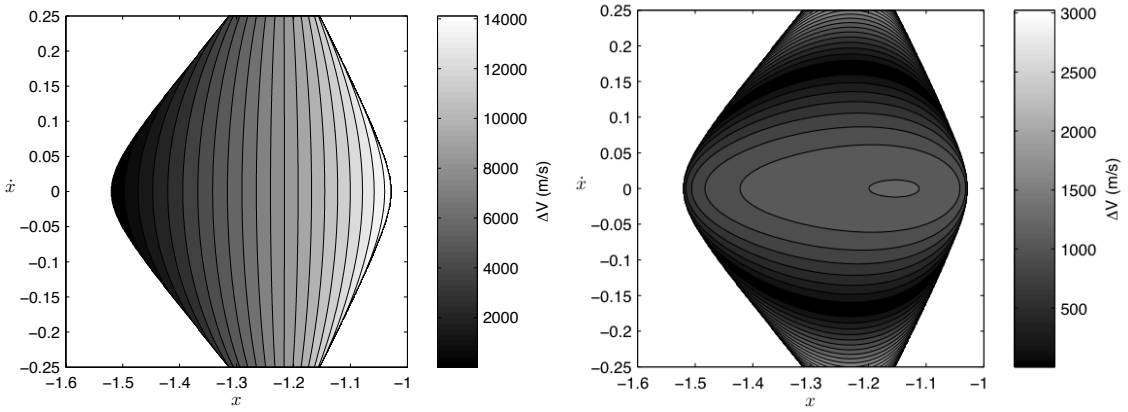

(a) $+\dot{y}$ case in the Jupiter-Ganymede System

(b) $-\dot{y}$ case in the Jupiter-Ganymede System

Figure 8. Theoretical ΔVs required for combinations of x and $\dot{x}$ at different points. C = 3.0068 in the Jupiter-Ganymede system and C = 3.0024 in the Jupiter-Europa System.

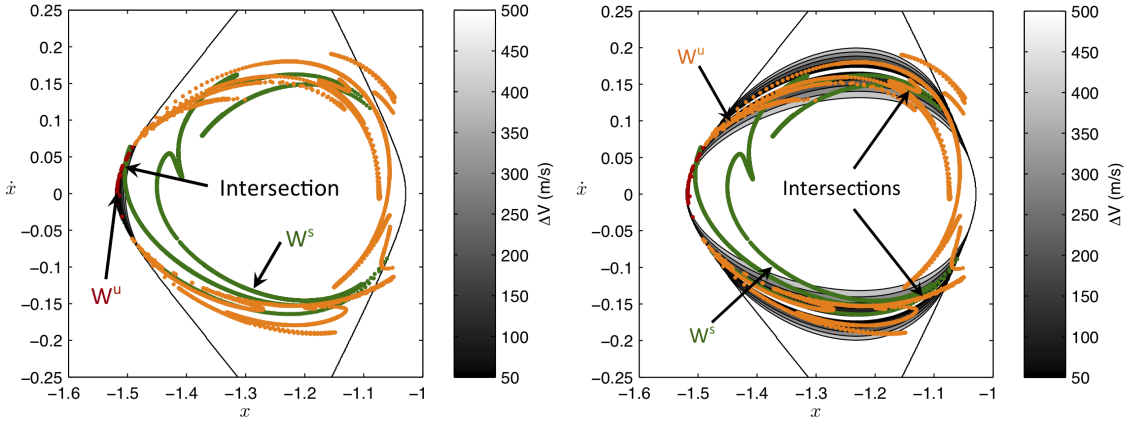

(a) $+\dot{y}$ case in the Jupiter-Ganymede System

(b) $-\dot{y}$ case in the Jupiter-Ganymede System

Figure 9. Theoretical ΔVs required for combinations of x and $\dot{x}$ at different points compared to the possible intersections of the invariant manifolds. C = 3.0068 in the Jupiter-Ganymede system and C = 3.0024 in the Jupiter-Europa System.

5:7 orbit occur in this region, and an intersection with relatively low ΔV does exist in this region. In Figure 9(b), the contours are appropriate for comparison with the orange points with $\dot{y} < 0$. A number of different potential intersections may be found in this region as well. After examining both plots, several potential intersections shown in the plot may be selected. These include intersections with ΔVs of approximately 101.6 m/s, 71.9 m/s and 66.7 m/s.

Factors other than the ΔV can play into the selection of the appropriate trajectory, so it is useful to examine some of the resulting trajectory segments directly. In each case, the trajectory on the invariant manifolds of the respective resonant orbits represented by the intersection in the Poincaré section may be integrated forward and backward in time in the appropriate system. Because an intersection is computed which is slightly different from the precomputed nearby trajectory, the trajectory needs to be recomputed. In each case, the invariant manifold trajectory will theoretically approach the resonant orbit asymptotically as the integration proceeds. Practically speaking, the trajectory will come close enough to the resonant orbit at some point to say

that it has reached the desired resonance. In order to connect the trajectory segments together, the trajectories are currently integrated until they come close to the desired resonance. The connections are currently limited to those that occur at Σ, but this is a limitation that is simply a limitation of the current algorithm and may be removed in the future. In the case of resonant orbits that have intersections at Σ that are not perpendicular to the surface of section, it is important to keep in mind the type of intersection that occurs when patching different invariant manifold segments.

The invariant manifold segments integrated forward and backward from the intersection are shown in Figure 10. The W^u trajectories of the 7:5 orbit are integrated backward from the intersection in the Jupiter-Ganymede frame, and the W^s trajectories of the 5:7 orbit are integrated forward from the intersection in the Jupiter-Europa frame. The case with a 101.6 m/s ΔV in Figures 10(a) and 10(d) is interesting for several reasons. The initial condition in the Jupiter-Ganymede frame on the 7:5 orbit integrated forward from that point is labeled, and the final point is the leftmost point on the figure. It can be seen from this figure that the last point occurs on the outermost point on the loop, explaining why the velocity in the Poincaré section is positive. This point is one of the few locations where it is positive in the Jupiter-Ganymede frame for an interior resonant orbit. Comparing the various cases provides additional insight into the selection of the appropriate trajectory. The 71.9 m/s case has many more revolutions in both the Jupiter-Ganymede and Jupiter-Europa rotating frames. The 66.7 m/s case ties in more directly to the 7:5 orbit in the Jupiter-Ganymede system, but takes a little more time than the 101.6 m/s case in the Jupiter-Europa system. Both the 71.9 m/s and the 66.7 m/s cases are patched together at a smaller distance from Jupiter when compared to the 101.6 m/s case.

COMPUTATION OF THE RESONANT SEQUENCE WITH THE PATCHPOINT ΔV

Now that several suitable trajectories to use in patching the two systems have been found, the next step is to search for resonant pathways that allow the spacecraft to travel from a resonance near Ganymede to a resonance near Europa. Anderson and Lo[20] examined several potential resonance transition sequences in the Jupiter-Europa system at different energies and showed that they could be differentially corrected to nearly continuous trajectories with minimal ΔV. Lantoine et al.[11] examined several different sequences, the shortest of which was a 5:4 – 4:3 – 7:5 sequence in the Jupiter-Ganymede system (at C = 3.0068) followed by a 5:7 – 3:4 – 7:9 – 5:6 sequence in the Jupiter-Europa system (at C = 3.0024). This sequence will be duplicated here to use as a test case for comparison with a numerically optimized trajectory.

The existence of this sequence depends on the existence of heteroclinic connections between the various resonant orbits at the selected Jacobi constants in both systems. A sample of the Poincaré sections and some of the integrated trajectories in both the Jupiter-Ganymede and Jupiter-Europa systems are shown next. In each case a heteroclinic connection was found for the specified Jacobi constants. The Poincaré section showing the heteroclinic connection between the 5:4 and the 4:3 resonant orbit in the Jupiter-Ganymede system is shown in Figure 11. The 4:3 to 7:5 connection with the corresponding integrated trajectories are shown in Figure 12. The resonant orbits in each case are plotted as gray trajectories. The Poincaré sections showing the heteroclinic connections for the Jupiter-Europa portion of the trajectory are shown in Figure 13, while the trajectory plots are omitted to save space.

DIFFERENTIALLY CORRECTED TRAJECTORIES

The existence of the heteroclinic connections for each resonant sequence at the desired Jacobi constant indicates that a feasible pathway exists for the spacecraft to travel along the desired route. The heteroclinic connections do theoretically require each invariant manifold to approach or depart the relevant orbit asymptotically, but it was shown in Anderson and Lo[20] that for several resonances in the Jupiter-Europa system, the trajectory segments similar to those computed here may be used to construct a trajectory with minor discontinuities and ΔVs without having to travel along the asymptotic approaches. A similar approach is used here to show that the computed segments can be used to form a nearly continuous trajectory in each three-body system. The trajectories are then patched together with a ΔV at the chosen interface between the systems. See Anderson and Lo[20] for more specifics on the implementation of this procedure in a single system. In

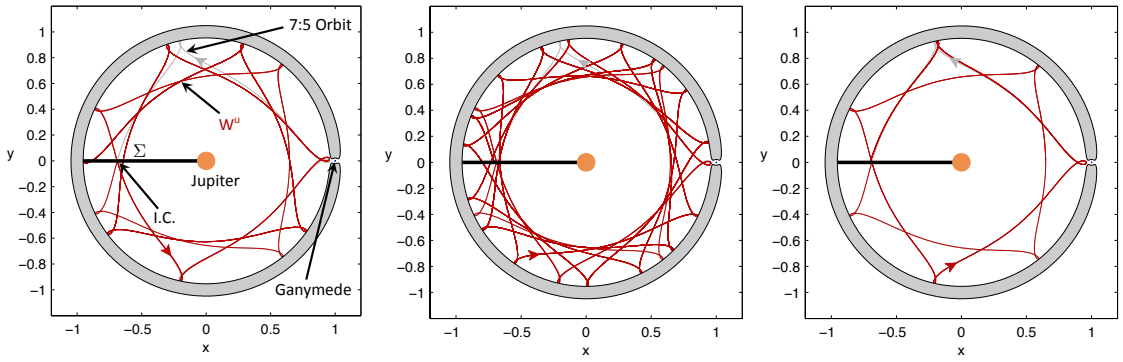

(a) ΔV = 101.6 m/s Case, Jupiter-Ganymede System (b) ΔV = 71.9 m/s Case, Jupiter-Ganymede System (c) ΔV = 66.7 m/s Case, Jupiter-Ganymede System

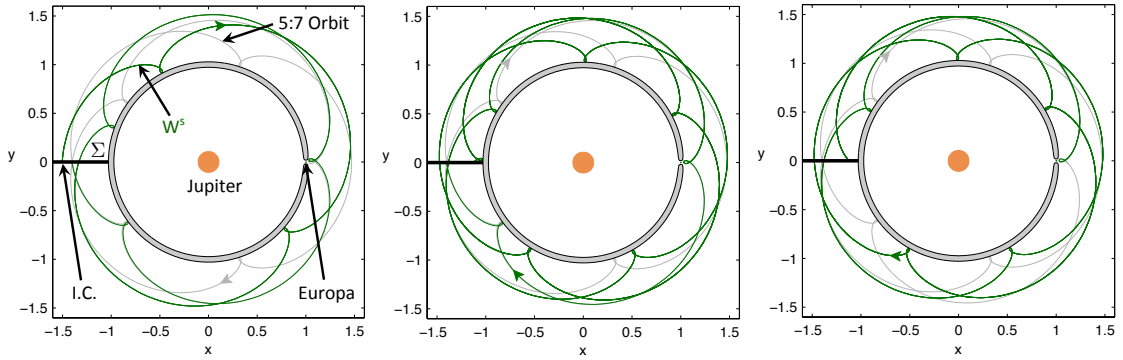

(d) ΔV = 101.6 m/s Case, Jupiter-Europa System (e) ΔV = 71.9 m/s Case, Jupiter-Europa System (f) ΔV = 66.7 m/s Case, Jupiter-Europa System

Figure 10. Integration of points on the Poincaré section corresponding to the W^u of the 7:5 orbit in the Jupiter-Ganymede frame backward in time and a point on the W^s of the 5:7 orbit in the Jupiter-Europa frame forward in time. C = 3.0068 in the Jupiter-Ganymede system and C = 3.0024 in the Jupiter-Europa System. The trajectories in the Jupiter-Europa system are all traveling toward the 5:7 resonant orbit (gray), and the trajectores in the Jupiter-Ganymede system are all traveling from the 7:5 resonant orbit (gray).

brief, the end points are held constant in position, and the velocity is allowed to vary. It does vary somewhat for the cases shown here which has some effect on the ΔV, but the overall pathway remains the same. Future work will focus on the differential corrections process and targeting the end conditions more specifically.

Two cases were converged in the differential corrector, and the overall characteristics of the resulting trajectories are summarized here. The trajectories for the 101.6 m/s case are plotted in their respective rotating frames in Figure 14. The Jupiter-Ganymede portion was converged to a point so that the sum of all position discontinuites were 0.004 m and the sum of all velocity discontinuities were 6.0 $\times 10^{-6}$ m/s. The Jupiter-Europa differentially corrected trajectories had similar discontinuities. The connecting patchpoint may be most clearly seen in the Jupiter-Europa frame as the leftmost point on the trajectory. The resonance transitions are more easily observed by looking at the periods over time. The time histories of the normalized two-body osculating period along the trajectory in both systems is given in Figure 15. The passage through various resonances can be observed by examining the normalized periods in each system compared to the period of a two-body resonance. In the Jupiter-Ganymede system, the 5:4 (period = 0.8), 4:3 (period = 0.75), and 7:5 (period = 0.714) segments are visible and bounded by flybys. It also appears that the invariant manifold trajectories may go through additional resonances as they transition between the computed resonant

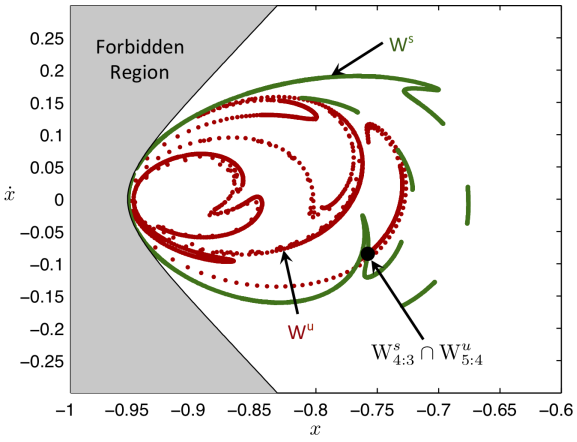

(a) Poincaré Section

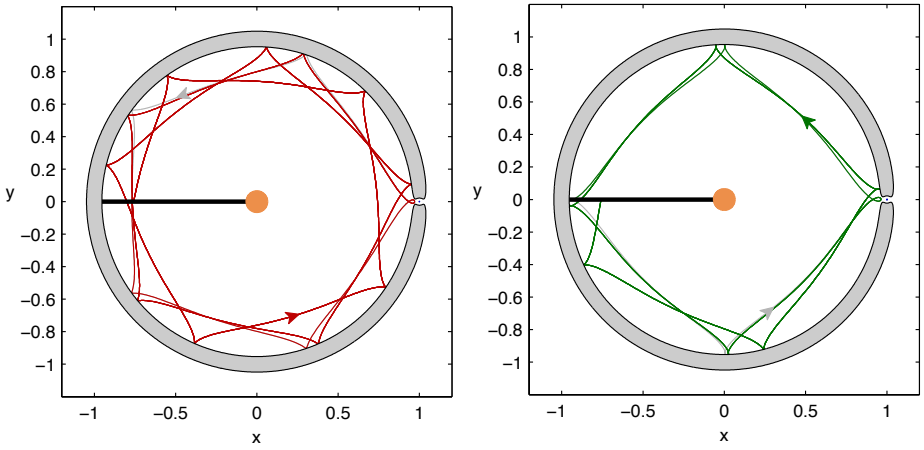

(b) 5:4 W^u Trajectory

(c) 4:3 W^s Trajectory

Figure 11. Poincaré section and configuration plots showing the W^u of the 5:4 resonant orbit and the W^s of the 4:3 resonant orbit in the Jupiter-Ganymede system at C = 3.0068. The selected heteroclinic connection is indicated with a black point in the Poincaré section.

orbits. In the Jupiter-Europa system, the 5:7 (period = 1.4), 3:4 (period = 1.33), 7:9 (period = 1.29), and 5:6 (period = 1.2) segments can be observed. Finally, a period change may also be observed when transitioning between the patchpoint connecting the systems. The TOF of this trajectory including both segments in total is approximately 491.7 days. The ΔV at the patchpoint for this solution after the differential correction was actually slightly lower than the predicted ΔV at 100.5 m/s.

The second case that was differentially corrected was the 66.7 m/s case. From the computed segments, it would be expected that this case would have a lower ΔV in addition to a lower TOF. The differentially corrected trajectories in both systems are shown in Figure 16. The Jupiter-Ganymede portion was converged to a point where the sum of the position patchpoint discontinuities were 0.004 m, and the sum of the velocity patchpoint discontinuities were 5.0 $\times 10^{-6}$ m/s. The Jupiter-Europa trajectory converged to lower tolerances than these. The converged trajectories are similar to the previous case, but an additional loop at the outer resonance may be observed in the Jupiter-Europa system. The two-body osculating periods are shown in Figure 17, and they show a similar transition as the previous case since the majority of the segments are the same. The period at the connecting patchpoint in this case is lower which makes it closer to the lower desired periods in the subsequent resonances. As expected the total TOF of the trajectory was approximately 486.6

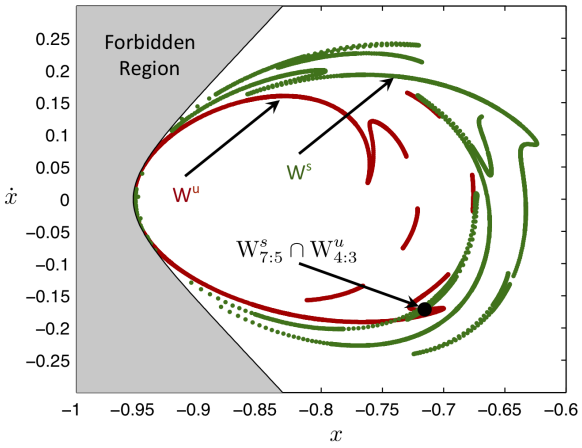

(a) Poincaré Section

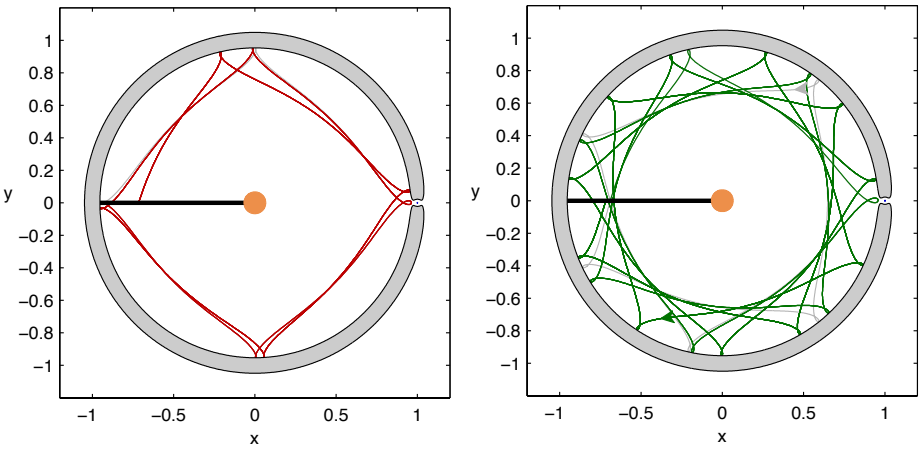

(b) 4:3 W^u Trajectory

(c) 7:5 W^s Trajectory

Figure 12. Poincaré section and configuration plots showing the W^u of the 4:3 resonant orbit and the W^s of the 7:5 resonant orbit in the Jupiter-Ganymede system at C = 3.0068. The selected heteroclinic connection is indicated with a black point in the Poincaré section.

days, 5.1 days less than the 101.6 m/s case. The converged ΔV was 71.9 m/s, which is somewhat higher than the predicted ΔV.

Compared to the cases using the same resonant path obtained using numerical optimization in Lantoine et al.[11] these results represent a significant savings in ΔV at the expense of increased TOF. Lantoine et al.[11] produced two cases with this resonant path. They included one with a ΔV of 125.9 m/s and a TOF of 119 days and one with a ΔV of 179.2 m/s and a TOF of 149 days. The lowest ΔV of all of their cases with a different resonant sequence was 55.5 m/s with a TOF of 227 days. Future work will include developing trajectories that match this longer resonant sequence. Keep in mind that the current results have been generated by simply using the dynamics, and a further step would be to place them into an optimizer to determine if further improvements in ΔV are possible.

It is also worth noting that the majority of the asymptotic approaches to the resonant orbits are still retained in the current results, but it is possible to significantly shorten this approach by eliminating some of these segments. As a matter of convenience, all patchpoints between segments are currently computed at Σ. Often the trajectory approaches close enough to the trajectory much earlier on, and a significant portion of many

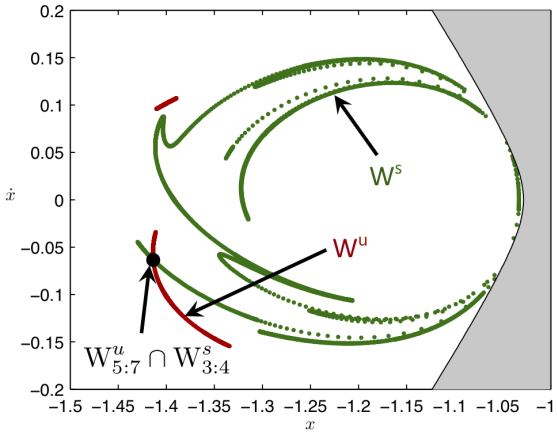

(a) 5:7 → 3:4 Heteroclinic Connection

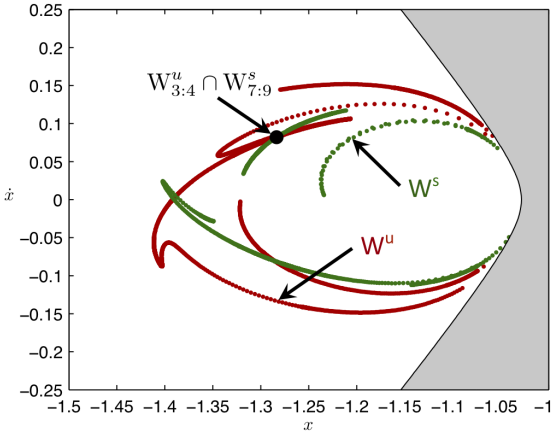

(b) 3:4 → 7:9 Heteroclinic Connection

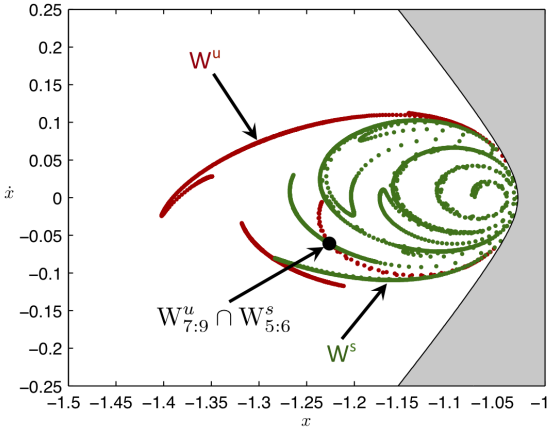

(c) 7:9 → 5:6 Heteroclinic Connection

Figure 13. Poincaré sections showing the W^u and W^s of the labeled orbits in the same order that the resonances are given. The points are computed in the Jupiter-Europa system, and C = 3.0024 in these plots.

revolutions may be dropped out if this is factored in. One effect on the ΔV magnitude is the placement of the ΔV. Currently these are also constrained to occur at Σ, but if the maneuver placement is allowed to vary, this may result in significant savings. There are areas for specific improvements, but the overall feasibility of the basic method in terms of the potential ΔVs that may be obtained has been shown.

Finally, optimizers generally allow maneuvers to exist at multiple points along the trajectory, and the Jacobi constant is allowed to vary as the ΔVs occur. So far the trajectories in each system have been constrained to remain at the same Jacobi constant. It is worth examining briefly the effect of changing the Jacobi constant on the procedure.

VARYING THE JACOBI CONSTANT WITH EACH SEGMENT

Rather than keeping the Jacobi constant the same within each system, it is possible to change the Jacobi constant with each segment. In other words, a ΔV will be performed between each trajectory segment. This happens naturally with typical optimization algorithms that place maneuvers along the trajectory at various points and optimize their location and magnitude to obtain the resulting trajectory. Therefore, the trajectory resulting from this dynamical systems technique may match the trajectory obtained from typical optimization

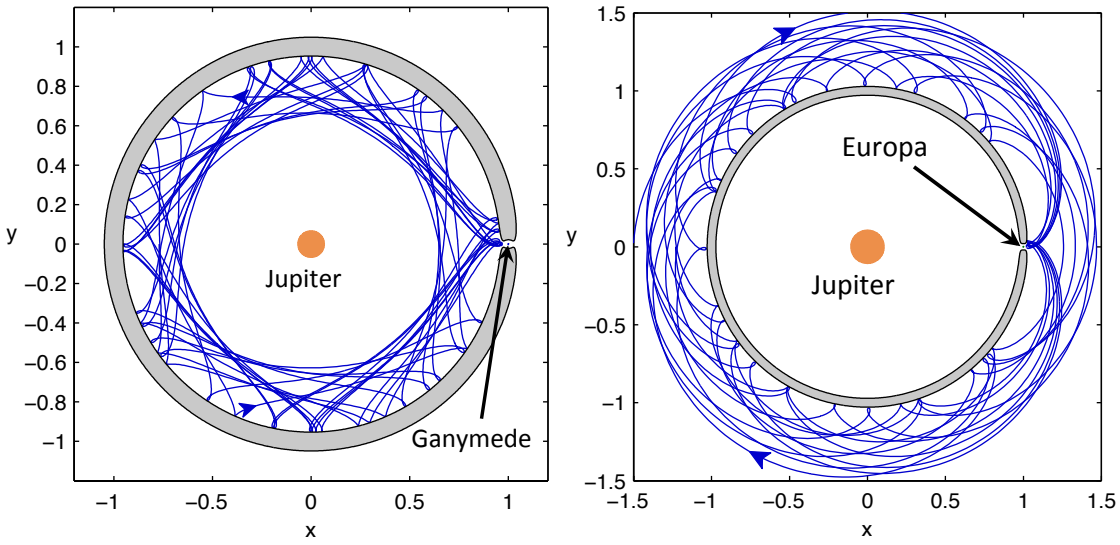

(a) Jupiter-Ganymede System, C = 3.0068

(b) Jupiter-Europa System, C = 3.0024

Figure 14. Differentially corrected trajectories in the rotating frame in each system for the ΔV = 101.6 m/s case

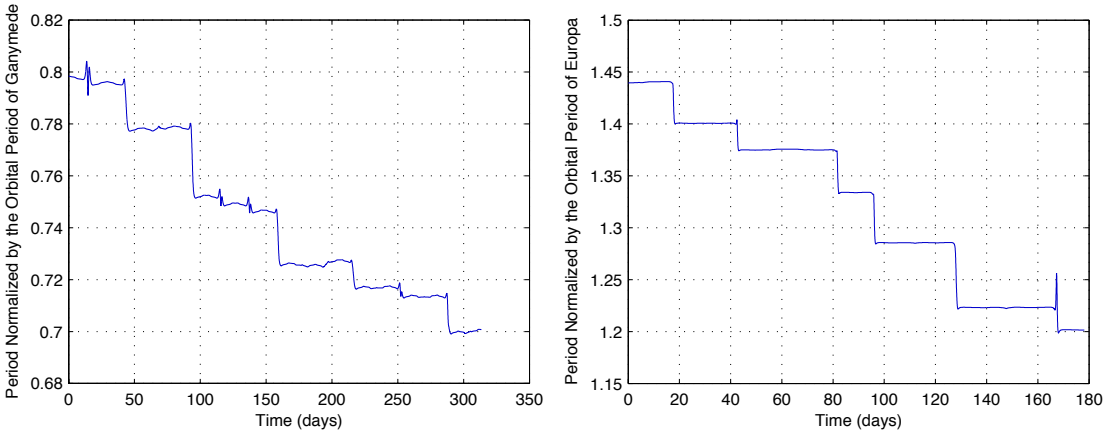

(a) Periods normalized by Ganymede's orbital period, C = 3.0068, Jupiter-Ganymede System, TOF $\approx$ 313.5 days

(b) Periods normalized by Europa's orbital period, C = 3.0024, Jupiter-Europa System, TOF $\approx$ 178.2 days

Figure 15. Normalized periods over time for each trajectory segment for the ΔV = 101.6 m/s case

algorithms more closely. While the Jacobi constant may be changed, choosing the Jacobi constant for each segment becomes an interesting problem. One particular case will be examined here to explore some of the potential trades.

For the case selected here, it is assumed that the Jupiter-Ganymede trajectory at C = 3.0068 is patched into the Jupiter-Europa system at a Jacobi constant of C = 3.0. A ΔV then occurs at the next segment to change the Jacobi constant to the target value of C = 3.0024. By comparing the Poincaré sections at C = 3.0024 and C = 3.0 in Figures 7(a) and 7(b) a few possible advantages to this approach might be seen. The first is that the stable manifolds have expanded for the lower Jacobi constant, and additional potential intersections or trajectory options are available. The ΔV equivalent to the C = 3.0024 case is now 76.2 m/s. Next, it is possible to jump from C = 3.0 to C = 3.0024 in the transition from the 5:7 resonance to the 3:4 resonance.

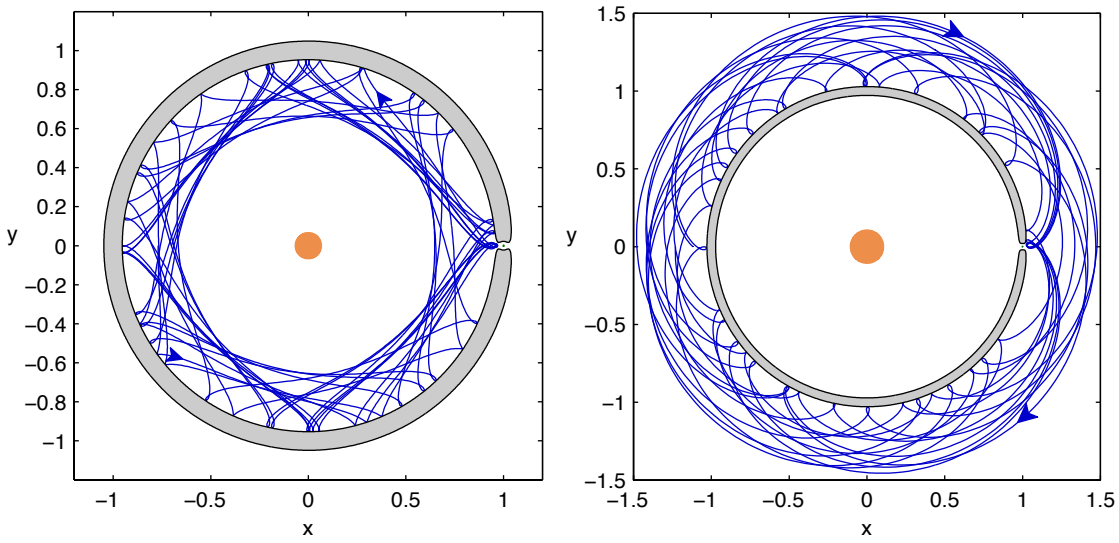

(a) Jupiter-Ganymede System, C = 3.0068

(b) Jupiter-Europa System, C = 3.0024

Figure 16. Differentially corrected trajectories in the rotating frame in each system for the ΔV = 66.7 m/s case

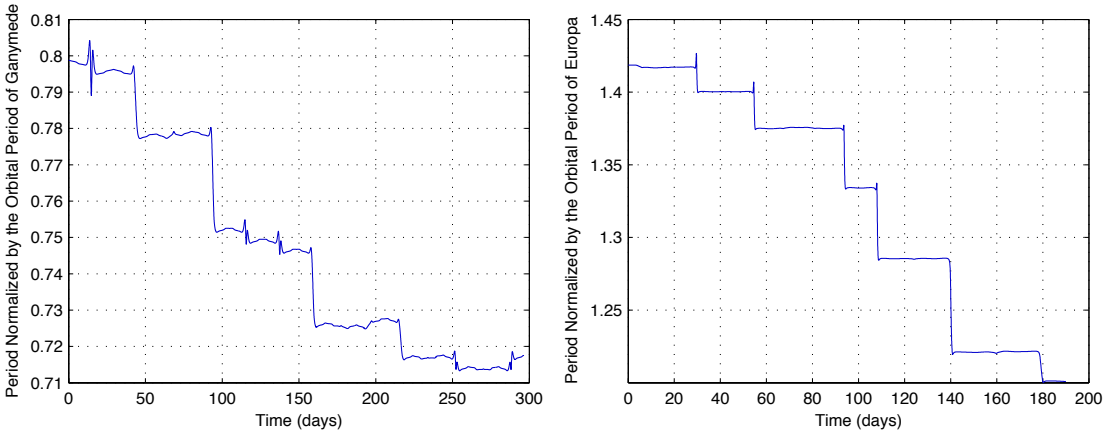

(a) Periods normalized by Ganymede's orbital period, C = 3.0068, Jupiter-Ganymede System, TOF $\approx$ 296.6 days

(b) Periods normalized by Europa's orbital period, C = 3.0024, Jupiter-Europa System, TOF $\approx$ 190.0 days

Figure 17. Normalized periods over time for each trajectory segment for the ΔV = 66.7 m/s case

The corresponding Poincaré section is shown in Figure 18, and it can be seen that several different options exist to transfer between the resonances. One of the faster routes gives a ΔV of 24.9 m/s which would result in a ΔV of approximately 101 m/s to transition to the desired Jacobi constant. This value is slightly lower than the value previously computed for transitioning in one jump, and it is possible that separating the Jacobi constant transitions over multiple segments could allow for more opportunities to reduce the overall ΔV. This process may also bring the total ΔV closer to the optimized values and allow for more options to reduce the transfer time.

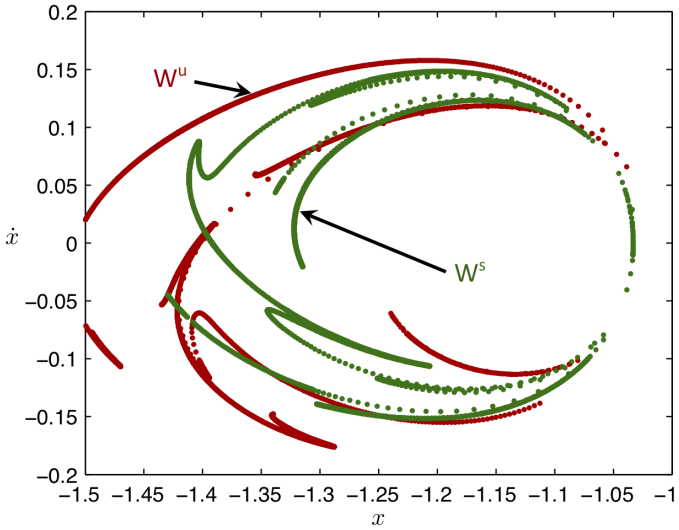

Figure 18. Poincaré Section at Σ in the Jupiter-Europa system. $W^u_{5:7}$ is computed at C = 3.0, and $W^s_{3:4}$ is computed at C = 3.0024.

CONCLUSIONS

A technique for patching CRTBP trajectories together using the intersections of the unstable and stable manifolds of resonant orbits has been implemented, and the practical aspects of designing a tour using this technique have been explored. It was shown that a trajectory traveling between a resonant orbit near Ganymede in the Jupiter-Ganymede system to a resonant orbit near Europa in the Jupiter-Europa system may be feasibly designed using these techniques in combination with the computation of heteroclinic connections of the resonant orbits in the sequence. The differential correction of two sample trajectories showed that the ΔV predicted from these techniques gives a prediction of the values obtained when the two CRTBPs are patched.

It has also been shown that the trajectories produced from a basic knowledge of the dynamics via the invariant manifolds of unstable resonant orbits produce initial results that are comparable in ΔV to optimized solutions. These trajectories currently have long TOFs, but it is expected that numerous segments of the trajectory may be culled to produce a significantly shorter TOF. Specific comparisons of these patched CRTBP results to trajectories with the same resonance transition sequence in the multi-body problem give a predicted ΔV of 71.9 m/s with a TOF of 486.6 days versus 125.9 m/s with a TOF of 119 days for the optimized solution from Lantoine et al.[11] Future comparisons will be made to their alternative resonant orbit sequence that produced a ΔV of 55.5 m/s, and more direct comparisons in the multi-body problem will be added. These results are significant considering that no optimization techniques were employed to obtain these trajectories. Finally, although the TOFs are significant, this is partly a factor of the low-energy regime under which the sample trajectories were generated. The formulation using the current technique is also applicable at lower Jacobi constants (higher energies) which should produce significantly lower TOFs. The feasibility of using these techniques to compute new solutions using insight into the dynamics has been demonstrated, showing the potential to obtain low-ΔV trajectories without the use of optimization techniques.

FUTURE WORK

Future work will focus on moving the current trajectory types into continuous versions in multi-body and ephemeris models. Additional differential correction constraints will be added, and the current techniques will be expanded to encompass a complete tour including additional moons and the final approach. The current initial guesses will also be supplied as initial guesses to optimization algorithms to evaluate any improvements in convergence. Eventually, similar techniques can be applied to low-thrust trajectories.

ACKNOWLEDGEMENTS

The author would like to thank Martin Lo for his support and helpful discussions on this topic, and he would like to thank Gregory Lantoine for his useful thoughts on the problem. He would also like to thank Jon Sims and Anastassios Petropoulos for their helpful comments and reviews of this paper. The research presented here has been carried out at the Jet Propulsion Laboratory, California Institute of Technology, under a contract with the National Aeronautics and Space Administration. Funding for this research came from AMMOS/MGSS under the "Tour and Endgame Design using Invariant Manifolds" study.

REFERENCES

[1] M. Okutsu, T. J. Debban, and J. M. Longuski, "Tour Design Strategies for the Europa Orbiter Mission," *Advances in the Astronautical Sciences, Astrodynamics* (D. B. Spencer, C. C. Seybold, A. K. Misra, and R. J. Lisowski, eds.), Vol. 109, Part III, San Diego, California, American Astronautical Society, Univelt Inc., 2001, pp. 2269 – 2284.

[2] N. J. Strange and J. M. Longuski, "Graphical Method for Gravity-Assist Trajectory Design," *Journal of Spacecraft and Rockets*, Vol. 39, January-February 2002, pp. 9–16.

[3] S. Campagnola and R. Russell, "Endgame Problem Part 2: Multibody Technique and the Tisserand-Poincare Graph," *Journal of Guidance, Control, and Dynamics*, Vol. 33, No. 2, 2010, pp. 476–486.

[4] K. W. Kloster, A. E. Petropoulos, and J. M. Longuski, "Europa Orbiter Tour Design with Io Gravity Assists," *Acta Astronautica*, Vol. 68, 2010, pp. 931–946.

[5] E. Bollt and J. D. Meiss, "Targeting Chaotic Orbits to the Moon through Recurrence," *Physics Letters A*, Vol. 204, August 28 1995, pp. 373–378.

[6] C. G. Schroer and E. Ott, "Targeting in Hamiltonian Systems that have Mixed Regular/Chaotic Phase Spaces," *Chaos*, Vol. 7, December 1997, pp. 512–519.

[7] E. Belbruno and B. Marsden, "Resonance Hopping in Comets," *Astronomical Journal*, Vol. 113, No. 4, 1997, pp. 1433–1444.

[8] M. Lo and S. Ross, "Low Energy Interplanetary Transfers Using Invariant Manifolds of L1, L2, and Halo Orbits," *Advances in the Astronautical Sciences, Spaceflight Mechanics* (J. W. Middour, L. L. Sackett, L. A. D'Amario, and D. V. Byrnes, eds.), Vol. 99, Part II, San Diego, California, American Astronautical Society, Univelt Inc., 1998, pp. 551–562.

[9] W. S. Koon, M. W. Lo, J. E. Marsden, and S. D. Ross, "Heteroclinic Connections between Periodic Orbits and Resonance Transitions in Celestial Mechanics," *Chaos*, Vol. 10, June 2000, pp. 427–469.

[10] K. C. Howell, B. Marchand, and M. W. Lo, "Temporary Satellite Capture of Short-Period Jupiter Family Comets from the Perspective of Dynamical Systems," *The Journal of the Astronautical Sciences*, Vol. 49, October-December 2001, pp. 539–557.

[11] G. Lantoine, R. P. Russell, and S. Campagnola, "Optimization of Low-Energy Resonant Hopping Transfers between Planetary Moons," *Acta Astronautica*, Vol. 68, April-May 2011, pp. 1361–1378.

[12] S. D. Ross and D. J. Scheeres, "Multiple Gravity Assists, Capture, and Escape in the Restricted Three-Body Problem," *Siam Journal On Applied Dynamical Systems*, Vol. 6, 2007, pp. 576–596.

[13] R. L. Anderson and M. W. Lo, "A Dynamical Systems Analysis of Planetary Flybys and Approach: Ballistic Case," *The Journal of the Astronautical Sciences*, Vol. 58, April-June 2011, pp. 167–194.

[14] M. W. Lo, R. L. Anderson, G. Whiffen, and L. Romans, "The Role of Invariant Manifolds in Low Thrust Trajectory Design (Part I)," *Space Flight Mechanics: Proceedings of the 14th AAS/AIAA Space Flight Mechanics Meeting held February 8-12, 2004, Maui, Hawaii* (S. L. Coffey, A. P. Mazzoleni, K. K. Luu, and R. A. Glover, eds.), Vol. 119 of *Advances in the Astronautical Sciences*, San Diego, California, American Astronautical Society, Univelt Inc., 2004, pp. 2971–2990.

[15] R. L. Anderson and M. W. Lo, "The Role of Invariant Manifolds in Low Thrust Trajectory Design (Part II)," *AIAA/AAS Astrodynamics Specialist Conference*, No. Paper AIAA 2004-5305, Providence, Rhode Island, August 16-19 2004.

[16] R. L. Anderson and M. W. Lo, "Dynamical Systems Analysis of Planetary Flybys and Approach: Planar Europa Orbiter," *Journal of Guidance, Control, and Dynamics*, Vol. 33, November-December 2010, pp. 1899–1912.

[17] M. W. Lo, R. L. Anderson, T. Lam, and G. Whiffen, "The Role of Invariant Manifolds in Low Thrust Trajectory Design (Part III)," *AAS/AIAA Astrodynamics Specialist Conference*, No. Paper AAS 06-190, Tampa, Florida, January 22-26 2006.

[18] R. L. Anderson and M. W. Lo, "Role of Invariant Manifolds in Low-Thrust Trajectory Design," *Journal of Guidance, Control, and Dynamics*, Vol. 32, November-December 2009, pp. 1921–1930.

[19] R. L. Anderson, *Low Thrust Trajectory Design for Resonant Flybys and Captures Using Invariant Manifolds*. PhD thesis, University of Colorado at Boulder, http://ccar.colorado.edu/~rla/papers/andersonphd.pdf, 2005.

[20] R. L. Anderson and M. W. Lo, "Flyby Design using Heteroclinic and Homoclinic Connections of Unstable Resonant Orbits," *21st AAS/AIAA Space Flight Mechanics Meeting*, No. AAS 11-125, New Orleans, Louisiana, February 13-17 2011.

[21] G. Lantoine and R. L. Anderson, "Evaluation of Initial Guess Strategies for Low-Energy Resonant Flybys," *JPL R&TD Poster Conference*, Pasadena, California, November 7 2012.

[22] R. L. Anderson, "Approaching Moons from Resonance via Invariant Manifolds," *22nd AAS/AIAA Space Flight Mechanics Meeting*, No. AAS 12-136, Charleston, South Carolina, January 29 - February 2 2012.

[23] R. L. Anderson and M. W. Lo, "Spatial Approaches to Moons from Resonance Relative to Invariant Manifolds," *63rd International Astronautical Congress*, No. IAC-12.C1.7.4, Naples, Italy, International Astronautical Federation, October 1-5 2012.

[24] T. M. Vaquero Escribano, "Poincaré Sections and Resonant Orbits in the Restricted Three-Body Problem," Master's thesis, Purdue University, West Lafayette, Indiana, May 2010.

[25] M. Vaquero and K. C. Howell, "Poincaré Maps and Resonant Orbits in the Circular Restricted Three-Body Problem," *AAS/AIAA Astrodynamics Specialist Conference*, No. AAS 11-428, Girdwood, Alaska, July 31 - August 4 2011.

[26] M. Vaquero and K. C. Howell, "Design of Transfer Trajectories Between Resonant Orbits in the Restricted Three-Body Problem with Application to the Earth-Moon System," *1st IAA/AAS Conference on the Dynamics and Control of Space Systems*, Porto, Portugal, March 19-21 2012.

[27] V. Szebehely, *Theory of Orbits: The Restricted Problem of Three Bodies*. New York: Academic Press, 1967.

[28] A. E. Roy and M. W. Ovenden, "On the Occurrence of Commensurable Mean Motions in the Solar System. The Mirror Theorem," *Monthly Notices of the Royal Astronomical Society*, Vol. 115, 1955, pp. 296–309.

[29] A. Miele, "Theorem of Image Trajectories in the Earth-Moon Space," *Astronautica Acta*, Vol. 6, No. 51, 1960, pp. 225–232.

[30] K. C. Howell and J. V. Breakwell, "Three-Dimensional, Periodic, 'Halo' Orbits," *Celestial Mechanics*, Vol. 32, January 1984, pp. 53–71.

[31] G. Gómez, A. Jorba, J. Masdemont, and C. Simó, "Study of the Transfer from the Earth to a Halo Orbit Around the Equilibrium Point L_1," *Celestial Mechanics and Dynamical Astronomy*, Vol. 56, August 1993, pp. 541–562.

[32] S. Wiggins, *Introduction to Applied Nonlinear Dynamical Systems and Chaos*, Vol. 2 of *Texts in Applied Mathematics*. New York: Springer-Verlag, 2nd ed., 2003, pp. 28-70.

[33] C. D. Murray and S. F. Dermott, *Solar System Dynamics*. Cambridge, United Kingdom: Cambridge University Press, 1999, pp. 421-428.

[34] W. S. Koon, M. W. Lo, J. E. Marsden, and S. D. Ross, "Resonance and Capture of Jupiter Comets," *Celestial Mechanics and Dynamical Astronomy*, Vol. 81, No. 1-2, 2001, pp. 27–38.

[35] M. Hénon, *Generating Families in the Restricted Three-Body Problem*, Vol. 52 of *Lecture Notes in Physics*. New York: Springer, 1997.

[36] W. S. Koon, M. W. Lo, J. E. Marsden, and S. D. Ross, "Constructing a Low Energy Transfer Between Jovian Moons," *Celestial Mechanics: Dedicated to Donald Saari for his 60th Birthday* (A. Chenciner, R. Cushman, C. Robinson, and Z. J. Xia, eds.), Vol. 292 of *Contemporary Mathematics*, American Mathematical Society, 2002, pp. 129–146.

[37] G. Gómez, W. S. Koon, M. W. Lo, J. E. Marsden, J. Masdemont, and S. D. Ross, "Invariant Manifolds, the Spatial Three-Body Problem and Space Mission Design," *Astrodynamics: Proceedings of the AAS/AIAA Astrodynamics Conference, July 30 - August 2, 2001, Quebec City, Quebec* (D. B. Spencer, C. C. Seybold, A. K. Misra, and R. J. Lisowski, eds.), Vol. 109 of *Advances in the Astronautical Sciences*, San Diego, California, American Astronautical Society, Univelt Inc., 2001, pp. 3–22.

[38] D. Blazevski and C. Ocampo, "Periodic Orbits in the Concentric Circular Restricted Four-Body Problem and Their Invariant Manifolds," *Physica D*, Vol. 241, 2012, pp. 1158–1167.

[39] W. S. Koon, M. W. Lo, J. E. Marsden, and S. D. Ross, *Dynamical Systems, the Three-Body Problem and Space Mission Design*. Springer, 2006.

[40] T. Parker and L. O. Chua, *Practical Numerical Algorithms for Chaotic Systems*. New York: Springer-Verlag, 1989, pp. 130-166.